X-RAY SOURCE CHARACTERISTICS AND DETECTION EFFICIENCIES OF PROTOTYPE LIXISCOPES

Stephen M. Seltzer
Center for Radiation Research
National Bureau of Standards

The most compact, portable arrangement of the Lixiscope consists of: (a) an X-ray-emitting radioactive source; (b) at some distance away, a scintillator screen, used to convert the X-ray image into a visible light image, which is coupled to (c) a microchannel-plate, visible-light, image-intensifier tube.

The devices used in the early feasibility study reported here are prototypes, whose performance characteristics have neither been comprehensively evaluated nor optimized. This paper will concentrate on the radioactive X-ray sources and scintillator screens used in our prototype units. This discussion will highlight some of those considerations necessary for the optimization of future Lixiscope designs, as well as provide some semi-quantitative information on the present prototype devices.

Radioactive Source

Success has been achieved with two commercially available radioactive sources, ^{125}I and ^{153}Gd, which decay by electron capture and which have emission spectra that appear to be particularly suitable for medical and dental diagnostic use. The ^{125}I sources were supplied by the Amersham-Searle Corp.* in their standard point-source configuration; the ^{153}Gd source was obtained from the Oak Ridge National Laboratory. In order to estimate the radiation emission characteristics of these finite, encapsulated sources, we must know the energies and intensities of radiation emitted by a single atom, and then correct for the effects of self-absorption in the finite source volume as well as attenuation in the source capsule window foils.

Radiation energies E and intensities n (probability per decay) are given in the first two columns of Table 1 for the decay of single atoms, for both ^{125}I (60.1 day half-life) and ^{153}Gd (242 day half-life). The data for ^{125}I were obtained from Reference 1, with some auxiliary information on energies[2] and relative intensities[3] of the X-rays emitted by the daughter ^{125}Te. For ^{153}Gd, the data were extracted from the Evaluated Nuclear Structure Data File (maintained by the Nuclear Data Group at the Oak Ridge National Laboratory), using auxiliary X-ray data[2,3] and a K-

shell fluorscence efficiency of 0.9184 for the ^{153}Eu daughter atom.

For estimating the reduction factor due to self-absorption in the source and attenuation in capsule windows, the following simplified model was used: (a) the active source volume was assumed to be a homogeneous, right-circular cylinder; (b) all photons were assumed to travel in a direction parallel to the cylinder axis and to cross perpendicularly through the window material; (c) scattering of photons was neglected. Although assumption (b) appears quite drastic, keep in mind that we are ultimately interested only in that portion of the emitted beam, tightly collimated about the source axis, in which the photons are nearly parallel to the axis. Concentrating all of the photons in that direction results in "effective" point-source emission data, and allows the usual factor $1/4\pi$ to account for the isotropic nature of the intrinsic emission.

With these assumptions, it can easily be shown that the reduction factor is given by

$$f = \frac{1 - e^{-\mu_s t_s}}{\mu_s t_s} e^{-\mu_w t_w},$$

where μ_s and μ_w are the photon total attenuation coefficients (for the photon energy of interest) for the source material and window materials, respectively, and where t_s and t_w are the thicknesses of the source and windows, respectively. Using data on μ from standard references[5-7], estimated emission intensities, $n' = fn$, for the finite, encapsulated sources considered are given in the last column of Table 1. From the data in Table 1, the average photon energy emitted by ^{125}I is ~28 keV; and for ^{153}Gd, the average energies are ~43 keV for the X-rays; and ~100 keV for the gamma rays.

Under the assumption that the source is a point source, we can then easily estimate the photon flux ϕ and exposure X at a distance r from the source:

$$\phi = 2.94 \times 10^6 \, NA/r^2$$
$$X = 0.0543 \, DA/r^2,$$

where ϕ is in cm^{-2}sec^{-1}, X is in mR sec^{-1}, r is in cm, and A is the source activity in mCi. In the above equations, the parameter N is the mean number of photons per disintegration that penetrate to distance r and is given** by $N \cong \sum_i n'_i \exp(-\mu_i r)$, where the summation is over the photon energies of interest,

---

**We have neglected scattering in the air.

11

Table 1. Estimated Radioactive Source Emission Characteristics*

^{125}I (60.1 d)	Energy (keV)	Mean number of photons per disintegration	
		Single atom	Effective point-source values for finite, encapsulated source
K X-rays:	27.20	0.398	0.378
	27.47	0.742	0.704
	30.94	0.073	0.070
	31.00	0.140	0.134
	31.70	0.045	0.043
Gamma ray:	35.46	0.067	0.064
^{153}Gd (242 d)			
K X-rays:	40.90	0.345	0.071
	41.54	0.623	0.133
	46.90	0.060	0.017
	47.04	0.116	0.033
	48.26	0.055	0.017
Gamma rays:	69.67	0.024	0.004
	97.43	0.295	0.111
	103.18	0.211	0.088

*For ^{125}I, based on an approximate estimate of self-absorption in 1-mm diam. × 1-mm thick C (density ≅ 1.5 g/cm³), and attenuation in a 0.5-mm Be capsule end-face (density = 1.85 g/cm³) and a 5-μm Ti window (density = 4.5 g/cm³).

For ^{153}Gd, based on an approximate estimate of self-absorption in

1-mm diam. × 1.6-mm thick Gd₂O₃ (density ≅ 5.2 g/cm³), and attenuation in a 10-mil Aℓ window (density = 2.7 g/cm³).

L X-rays, heavily absorbed in finite encapsulated source, are assumed absent.

and μ is the photon total attenuation coefficient in air. D is effectively the air kerma per disintegration due to photons that penetrate to distance r, and is given by $D = \sum_i n'_i E_i \mu^i_{en} \exp(-\mu_i r)$, where μ_{en} is the photon mass energy-transfer coefficient in air.

For the energies and distances of interest, we can neglect the attenuation in air and find

		N	D
^{125}I	X + γ	1.4	4.8
^{153}Gd	X	0.27	0.67
	γ	0.20	0.48

Using these results, estimates of the photon flux and exposure produced by sources of 50 mCi ^{125}I and 200 mCi ^{153}Gd are given in Table 2. The approximations made in obtaining these results make their reliability somewhat uncertain. We note, however, that exposure measurements made on these sources with field survey instruments agree with the predictions to within about 30%.*

The lower limit of the detected X-ray flux for which an imaged object can be recognized (the so-called quantum limit) is somewhat subjective, and depen-

dent on a number of factors which can vary greatly according to the task. As a guideline we can borrow an illustrative example used elsewhere[8]: a high-contrast, 0.1-mm object (5 ℓp/mm) whose quantum limit for real-time viewing is $\sim 10^5$ cm^{-2}sec^{-1}. Then consider this object behind ~ 5 cm of tissue, at a source-to-skin-distance of r = 2 cm.** For an attenuation factor of ~ 0.2 due to the tissue and a detection efficiency of ~ 0.5, we need an incident flux of 10^5 (7 cm/2 cm)²/(0.2×0.5) = $\sim 10^7$ cm^{-2}sec^{-1} for the high-contrast object. A more difficult task might require a flux of, say, $\sim 10^8$ cm^{-2}sec^{-1}. We see from Table 2 that we are just in this range with the present sources; that is, we are operating close to quantum limits.

Scintillator Screen

The detection efficiencies (the fraction of incident photons which suffer an interaction) for two scintillator screens are shown in Figure 1 as a function of photon energy. The rare-earth curve is representative of the Kodak Lanex Regular single screen used in the prototype device. The CsI curve corresponds to an ~ 180-μm CsI screen which has not yet been successfully tried. The curve for a bare X-ray film is included for reference. Indicated by arrows in

*These discrepancies may indicate a faulty characterization of the source matrix. Keep in mind also that the activity specified for the commercial sources were nominal values.

**A plastic spacer might be attached to the source holder to insure r ≥ 2 cm, in order to keep the skin exposure at tolerable levels.
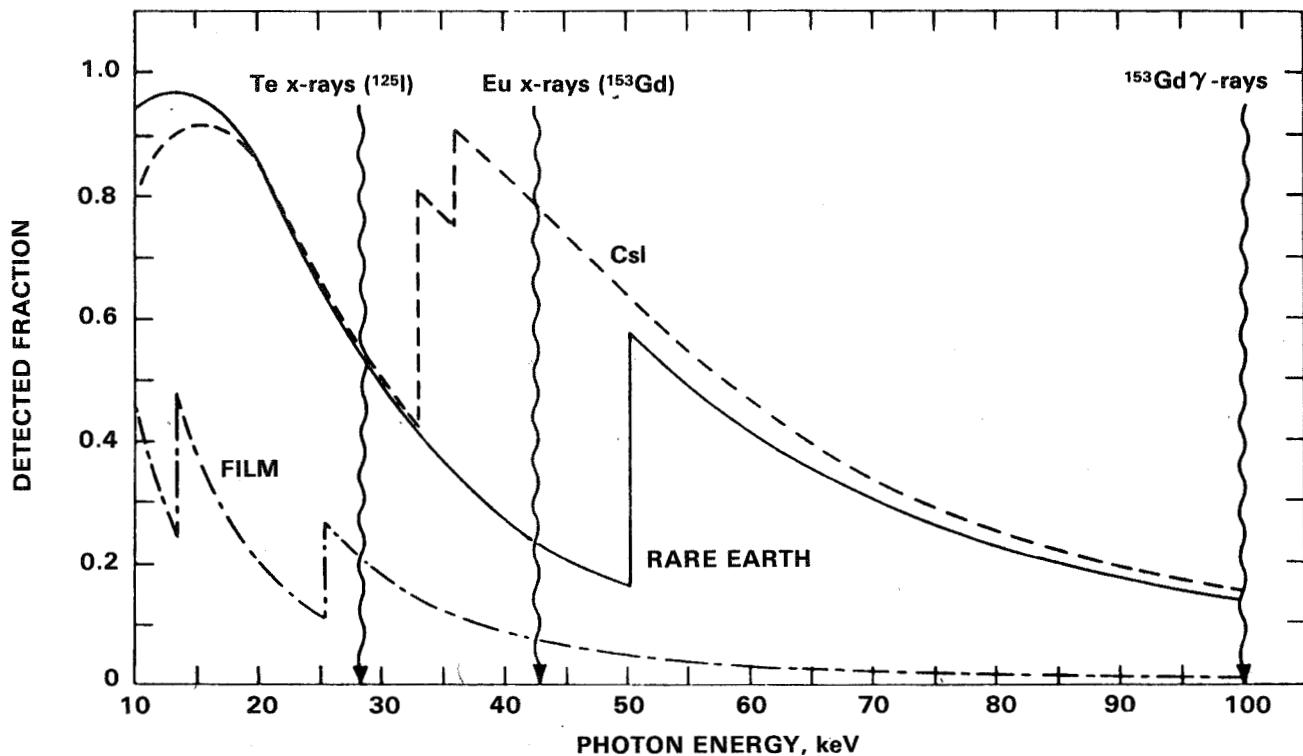
Figure 1. Detection Efficiency for Scintillator Screens, as a Function of Photon Energy. Energies of the photon components emitted by ^{125}I and by ^{153}Gd sources are indicated. The "rare earth" curve pertains to 55 mg/cm² of Gd_2O_2S behind 30 mg/cm² of C. The CsI curve corresponds to 80 mg/cm² of CsI behind 10 mg/cm² of Aℓ. The curve for film, 7 mg/cm² of AgBr, is shown for reference.

Table 2.   Estimated Photon Fluxes and Exposures from the Radioactive Sources*

r(cm)	50 mCi ^{125}I		200 mCi ^{153}Gd	
	ϕ (cm² sec⁻¹)	X(mR/sec)	ϕ_x (cm² sec⁻¹)	$X_{x+\gamma}$ (mR/sec)
2	5.1×10^7	3.3	9.8×10^7	3.1
5	8.2×10^6	0.52	1.6×10^7	0.50
10	2.1×10^6	0.13	3.9×10^6	0.12
20	5.1×10^5	0.033	9.8×10^5	0.031

*For ^{153}Gd, the exposure includes contributions from both the X- and gamma rays; the flux values include only the diagnostically useful X-rays.

13

Figure 1 are the energies of the ~28 keV X-rays from the ^{125}I source and the ~43 keV X-rays and ~100 keV gamma-rays from the [153]Gd source.

For the ^{125}I source, the detection efficiencies of the rare-earth screen and the proposed CsI screen are both ~55%. For the [153]Gd-source X-rays, the detection efficiency of the CsI screen (~80%) is roughly three times greater than that of the rare-earth screen (~25%). Also, for the case of the [153]Gd source, the CsI screen has the advantage that it detects the diagnostically useful 43-keV X-rays about 5 times more efficiently than the 100-keV gamma-rays which carry little information, and thereby constitute a background.

Because of the very high spatial resolution of the microchannel-plate intensifier tube, the resolution of the Lixiscope is largely governed by the resolution of the scintillator screen. Rough figures of merit can be estimated from available literature on modulation transfer functions (MTF's). The limiting resolution is sometimes defined as the frequency (ℓp/mm) at a modulation transfer of 0.04–0.05. Then, for the rare-earth screen, the resolution can be estimated[9] to be ~4 ℓp/mm, which is consistent with our observations. For a 180-μm mosaic CsI screen, the resolution may be expected[10] to be in the region of 2–3 ℓp/mm.

Other factors will affect the overall resolution of the system. For example, a finite-source spot size, a short source-to-object distance, and a non-negligible object-to-detector distance can combine to produce a significant penumbra and, consequently, a blurring of the image. In addition, eye blur in viewing the output image can reduce the apparent resolution. For this reason, magnifying the output image should improve its sharpness.

REFERENCES

1. M. J. Martin, Oak Ridge National Laboratory Publ. ORNL-5114 (1976).
2. J. A. Beardon, Rev. Mod. Phys. *31*, 1 (1967).
3. S. I. Salem, S. L. Panossian and R. A. Krause, Atomic Data and Nuclear Data Tables *14*, 91 (1974).
4. M. J. Martin, Nucl. Data Tables *8*, 1 (1970).
5. J. H. Hubbell, National Bureau of Standards Publ. NSRDS-NBS 29 (1969).
6. E. Storm and H. I. Israel, Nucl. Data Tables *7*, 565 (1970).
7. J. H. Hubbell, Rad. Res. *70*, 58 (1977).
8. H. Roehrig, M. Frost, R. Baker, S. Nudleman and P. Capp, Soc. Photo-Optical Instr. Engr. *78*, 102 (1976).
9. L. I. Yin, J. I. Trombka, S. M. Seltzer, R. L. Webber, M. R. Farr and J. Rennie, Soc. Photo-Optical Instr. Engr., *143*, 106 (1978).
10. S. P. Wang, C. D. Robbins and C. W. Bates, Jr., Soc. Photo-Optical Instr. Engr. *127*, 188 (1977).